J. Micromech. Microeng. **23** (2013) 055008 (10pp) doi:10.1088/0960-1317/23/5/055008

Creating large out-of-plane displacement electrothermal motion stage by incorporating beams with step features

Yong-Sik Kim[1,2,3], **Nicholas G Dagalakis**[1] **and Satyandra K Gupta**[2]

[1] Intelligent System Division, Engineering Laboratory, National Institute of Standards and Technology, 100 Bureau Dr. Gaithersburg, MD 20899, USA
[2] Department of Mechanical Engineering and Institute for Systems Research, University of Maryland, College Park, MD 20742, USA

E-mail: mk37do@gmail.com

Received 9 August 2012, in final form 4 March 2013
Published 26 March 2013
Online at stacks.iop.org/JMM/23/055008

Abstract
Realizing out-of-plane actuation in micro-electro-mechanical systems (MEMS) is still a challenging task. In this paper, the design, fabrication methods and experimental results for a MEMS-based out-of-plane motion stage are presented based on bulk micromachining technologies. This stage is electrothermally actuated for out-of-plane motion by incorporating beams with step features. The fabricated motion stage has demonstrated displacements of 85 μm with 0.4 μm (mA)$^{-1}$ rates and generated up to 11.8 mN forces with stiffness of 138.8 N m^{-1}. These properties obtained from the presented stage are comparable to those for in-plane motion stages, therefore making this out-of-plane stage useful when used in combination with in-plane motion stages.

(Some figures may appear in colour only in the online journal)

1. Introduction

In micro-electro-mechanical systems (MEMS), precise positioning of micro-objects finds important applications in biomedical research [1], micro-assembly [2], micro-grippers [3] and scanning probe microscopy [4]. Since the target objects are getting smaller, MEMS technologies have been applied to develop a wide variety of miniaturized motion stages [1, 3–5]. In many applications, the MEMS-based motion stages capable of generating both in-plane and out-of-plane (vertical) motions can provide additional positioning options and improved controllability. But realization of such a stage based on conventional MEMS processes is still challenging. This is due to the considerable difference in designs and fabrication methods between the in-plane and the out-of-plane actuation mechanisms. Additionally, the out-of-plane stages reported so far demonstrate relatively lower performance than in-plane stages. Therefore, it is necessary to develop a new out-of-plane motion stage that is equivalent to in-plane motion stages. This equivalence implies similar performances between in-plane and out-of-plane stages, such as motion range, force generation, stiffness and frequency response. For example, one of the commercial nanopositioners PI[4] NanoCube [6] has demonstrated its usefulness from its cubic-shaped workspace. This workspace comes from the similar motion range in both in-plane and out-of-plane directions, which is more practical than a skewed workspace in real applications. Many reported in-plane motion stages have motion ranges from 25 [7] to 60 μm [5] or more, while most out-of-plane motion stages are limited to less than 15 μm (e.g., 1.5 μm reported in [8], 3.5 μm reported in [7]). Additionally, similar force and stiffness scales are also desirable in many applications; in micromanipulation applications, the same stiffness level along multiple directions can reduce unwanted bending motions or distortions when interacting with stiff target objects. In

[3] Author to whom any correspondence should be addressed.

[4] Certain commercial equipment is identified in this paper to adequately describe the experimental procedure. Such identification does not imply recommendation or endorsement by the National Institute of Standards and Technology nor does it imply that the equipment identified is necessarily the best available for the purpose.

addition, similar fabrication methods to in-plane stages are also another requirement. Requiring special tools like wafer bonding [7] or focused ion beam (FIB) [8] for out-of-plane stages has been a major obstacle to expanding their applications. Thus, this paper focuses on the development of an out-of-plane MEMS motion stage that can provide equivalent performance to one of the existing in-plane stages and follows the same fabrication methods with the chosen in-plane stage.

There have been various approaches for out-of-plane motion stages. Among them, one of the most efficient methods is to utilize existing in-plane actuators. This method requires no additional effort on the actuator design and has an advantage to provide similar stiffness and motion range. However, in order to utilize an existing actuator, converting structures such as inclined planes [8] or polarity hinges [9, 10] are necessary. The gap and the friction from the motion direction converting mechanisms restrict the precision that can be achieved. One of the other simple methods for generating out-of-plane motion is rotating an in-plane actuator by 90° and then inserting it into a fixed base frame during the post-processing step [11]. Since the erected actuator is exactly the same as the in-plane one, these actuators can provide similar motion range and force. However, the manual rotation and assembly process make it difficult to ensure good quality over multiple devices and cannot be used in mass production situations.

Instead of utilizing existing in-plane actuators, dedicated out-of-plane actuators have also been developed based on widely used actuation methods such as electrostatic, electromagnetic and electrothermal. The electrostatic actuators are well known for their low power dissipation, fast frequency response and simple geometries [12]. Based on this actuation method, parallel plate [7, 12] and asymmetrical vertical combs [13] have been commonly used for out-of-plane motions. One of the parallel plate types demonstrated 3.5 μm out-of-plane motions [12], but requires two big parallel plates, which can require different fabrication methods such as a wafer bonding [7]. Asymmetrical combs for out-of-plane motions have a similar design to in-plane comb drives, but its motion range is relatively smaller than in-plane motion due to the limited area between electrodes [13]. Another candidate is the electromagnetic actuators which are based on the Lorentz force principle and have been implemented as a combination of micro-coils and magnetic fields [14–17]. These electromagnetic actuators have high bandwidth and also perform bidirectional displacement up to a few micrometers. The magnetic field for the actuator can be obtained through electroplating [15, 16], polymer deposition [17] and permanent magnets [4, 14]. Among them, the permanent magnets are stronger than the others, but are not compatible with MEMS fabrication processes. In addition, the magnetic field for one actuator can interfere with the other actuators, because it is difficult to isolate one magnetic field completely from the others. This can reduce the integration capability with other in-plane electromagnetic actuators.

As an alternative, electrothermal actuators have been utilized [5, 17, 18, 20] for their large forces (of the order of a few mN) and stiffness (of the order of tens of N m^{-1}), which are attractive in micro-manipulation applications. One of the commonly used out-of-plane electrothermal actuators is a cold and a hot arm that can generate out-of-plane motions up to 9 μm from the electrical resistance difference between the two arms [18]. This actuator is simple to fabricate and available for both in-plane and out-of-plane motions. But with this kind of actuator, it is difficult to generate linear motions. In order to generate a linear motion, symmetric beam designs with additional shapes like bridges or steps have been adapted to demonstrate 7 [20] to 14 μm [19] out-of-plane motions. The additional shapes have been fabricated mainly through surface micromachining technologies for multiple depositions and partial etchings. Contrary to surface micromachining technologies, bulk micromachining technologies have been rarely used for the out-of-plane structure due to its limited fabrication processes. However, there are many needs for the out-of-plane actuator based on bulk micromachining technologies, because this approach can provide stiffness and forces greater than those from surface micromachining technologies.

In this paper, an existing in-plane stage based on bulk micromachining has been selected as a target and a new electrothermally actuated out-of-plane motion stage has been designed to provide characteristics similar to the selected one including motion range, stiffness and force. The chosen motion stage can provide an in-plane displacement of 60 μm and a stiffness of 39.5 N m^{-1} [5, 32]. The basic design concept and its details are described in section 2. In order to achieve similar properties to the chosen in-plane stage, theoretical analyses and finite element analysis (FEA) were utilized and are explained in sections 3 and 4, respectively. The fabrication procedures for the out-of-plane motion stage are depicted in section 5. Experimental results including its range of motion, stiffness, frequency response and resistivity check are presented in section 6.

2. Design of the motion stage

In many MEMS electrothermal actuators, one commonly used electrothermal actuator is a bent-beam type or chevron type in-plane actuator [5, 21, 32] due to its simple structure and linear motion. This type of actuator is composed of aligned V-shaped beams pointing toward its actuation direction that convert thermal expansion of the beams into a linear motion. In this case, the bent beam angle plays an important role in determining its actuation direction. If this angle can be aligned toward a vertical direction, then this actuator can generate out-of-plane motion. There have been several designs to fabricate this out-of-plane bent beam through a step-bridge shape [19] or trench [22, 23]. But, many of them still have their own limitations such as smaller motion range and more complex fabrication processes than in-plane actuators due to lack of appropriate MEMS fabrication technologies.

The proposed actuator consists of four flat beams that have two steps at their ends and are connected at their center, as described in figure 1(*a*). When a current flows through the beam, it would generate a temperature rise by Joule heating and thermally expand. The height difference from the step features in the beam generates a bending moment from this

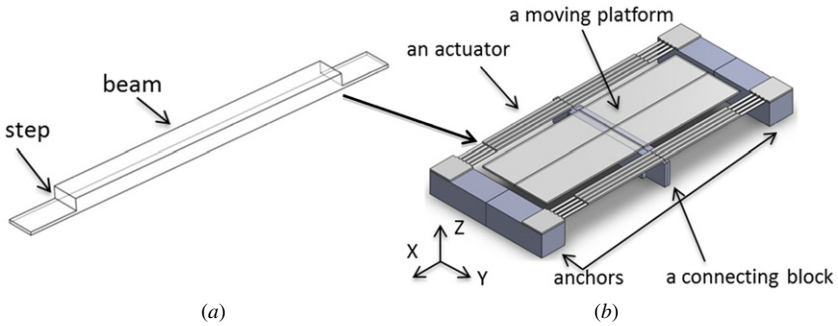

Figure 1. (*a*) A schematic illustration of a single beam with step features; (*b*) a 3D design of the motion stage actuated by the proposed two out-of-plane actuators that utilize four beams with step features (the device layer in gray and the handle layer in blue).

thermal expansion, which results in an upward or downward out-of-plane motion. By placing two steps at the ends of the beam, the bending moment is utilized for creating an upward out-of-plane displacement.

Based on this electrothermal actuator, a MEMS motion stage has been designed and is illustrated in figure 1(*b*), where the stage is composed of two out-of-plane electrothermal actuators and a moving platform. The actuators are indirectly connected to the moving platform through a connecting block to generate motions and are positioned symmetrically at both sides of the platform to compensate for any rotational motion. The moving platform is supposed to provide an interface or a base frame for external applications such as grippers or mirrors. The device is designed based on a silicon-on-insulator (SOI) wafer which is composed of two layers of silicon and an insulation layer between them. The insulation layer between them isolates the actuators from the moving platform, which makes the platform electrically and thermally isolated from the actuator. Main components such as actuators and the moving platform are located in the first layer of silicon, called a device layer, and the other components like anchors and the connecting block are in the second layer of silicon, called a handle layer. These layers and components are described in figure 1(*b*). Since the fabrication process for this stage is composed of pure etching steps, it can be fabricated based on bulk micromachining technologies, especially silicon-on-insulator multiuser multi-processes (SOI-MUMPs) [24].

3. Theoretical analysis

Figure 2(*a*) shows a schematic diagram of the beam in figure 1(*a*) for analysis. Two step features connect a lower portion of the beam to a fixed base. The force generated from the thermal expansion of the beam is denoted as P and P'. The free-body diagram of the beam is described in figure 2(*b*), where the step height from the action line of load P to the center line of the beam is denoted as e. The eccentric force P can be replaced with force P acting on the beam cross-sectional center and a moment M_a, $M_a = M_b = P_e$, as illustrated in figure 2(*c*). Since the lower portion of the beam is connected to a fixed base, the steps produce eccentric load which results in an upward out-of-plane motion. With a pinned–pinned boundary condition, $y(0) = 0$ and $y(L) = 0$, the analytic relationship for

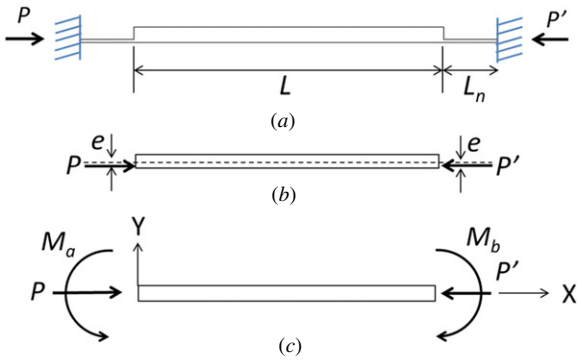

Figure 2. Diagrams for the beam analysis; (*a*) the schematic diagram of one beam of the actuator; (*b*) an eccentric load P from a thermal expansion of the beam; (*c*) a converted free-body diagram of the beam.

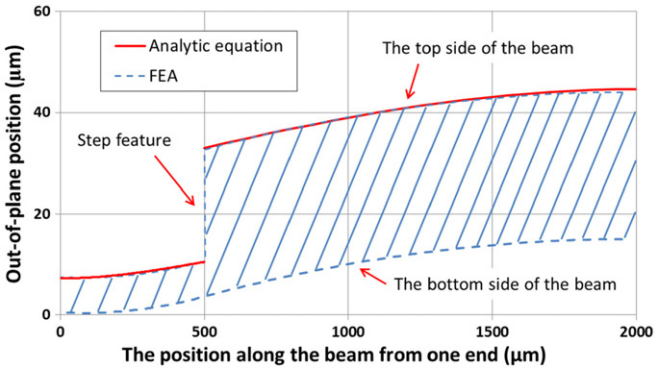

Figure 3. A comparison of out-of-plane deformation from equation (1) and FEA as a function of the position along the beam from one end.

the beam deformation profile can be expressed [25] as

$$y = e\left\{\tan\left(\sqrt{\frac{P}{EI}}\frac{L}{2}\right)\sin\left(\sqrt{\frac{P}{EI}}x\right) + \cos\left(\sqrt{\frac{P}{EI}}x\right) - 1\right\}, \quad (1)$$

where E is the Young modulus of silicon and I is the area moment of inertia of the beam. Based on equation (1) and the dimensions listed in table 1, the deformation profile of the actuator is calculated and plotted in figure 3, where this profile was verified by comparing with the profile from FEA.

The value of the maximum deflection y_{max} can be obtained at the middle of the beam ($x = L/2$) and can be expressed as

$$y_{max} = e\left\{\sec\left(\sqrt{\frac{P}{EI}}\frac{L}{2}\right) - 1\right\}. \quad (2)$$

Table 1. The design parameters in the actuator.

Components	Symbol	Design parameters	Dimensions (μm)
Beam	W	Width	33
	H	Height	30
	L	Length	3000
Step	L_n	Length	500
	e	Distance from the central line of the beam to the central line of the step	11

Table 2. Material properties of silicon [5].

Material properties	Value
Young's modulus	130 GPa
Poisson's ratio	0.28
Resistivity	$-4.72 \times 10^{-7}T + 4 \times 10^{-4}$ Ωm
Coefficient of thermal expansion	$3 \times 10^{-9}T + 3 \times 10^{-6}$ (/°C)
Thermal conductivity (T is in °C)	$5 \times 10^{-4}T^2 - 0.4706T + 164.15$ W (m °C)$^{-1}$
Yield strength	7 GPa

Equation (2) implies that the step depth (e), beam length (L) and the force (P) are the main parameters in determining the beam displacement performance. The longer L can produce a longer displacement, but this is vulnerable at buckling and also limited by the allowable chip area. The load P can be expressed from a classic beam theory as

$$P = 2\alpha\,\Delta T_{\text{ave}} EWH, \tag{3}$$

where α is the coefficient of thermal expansion of silicon, W is the beam width, H is the beam height and an average temperature rise over the beam ΔT_{ave} can be described [26] as

$$\Delta T_{\text{ave}} = \frac{V^2}{3k\rho} = \frac{2}{3}\Delta T_{\max}, \tag{4}$$

where k is the thermal conductivity of silicon, ρ is the resistivity of silicon and V is the driving electrical voltage applied to the actuator. The load P can be expressed as a function of temperature and this relationship is described in equations (3) and (4). In this case, the maximum P is also determined through the maximum allowable temperature $\Delta T_{\max}$, which causes silicon to deform permanently, which is 550 °C [27] or 800 °C [28, 29]. In this paper, 550 °C is selected as a temperature constraint.

Since the two parameters L and P are limited by the available chip area and thermal properties of silicon, the other design parameters e and L_n were investigated in the following FEA section to increase the performance of the actuator. Except for these design parameters, the remaining parameters of the beam have been selected based on this theoretical analysis and available resources; since commercially available SOI wafers are selected as a starting material which has a 30 μm thick device layer, the beam height (H) is set to be 30 μm. The beam width (W) is larger than the beam height (H) by 10% in order to prevent any in-plane deformation from starting prior to out-of-plane deformation. Since the longer beam is favorable at its maximum displacement, the beam length (L) is determined from the allowable area for the device. For the device reported in this paper, the total chip size is set to be less than 4 mm $\times$ 4 mm, so L is set as $L = 4$ mm $- 2L_n$. All parameters are described in table 1 with their corresponding values.

4. Finite element analysis

Commercial FEA software, ANSYS[4], is utilized to simulate the behaviors of the presented actuator and to find optimum values for the design parameters e and L_n. The actuator is made of silicon and its material properties are listed in table 2. An electric potential difference as electric excitation is applied between both ends of the actuator, and this analysis includes electric, thermal and structural beam response. For thermal analysis, both ends of the actuator beam are assumed to be linked directly to a heat sink which is at room temperature (20 °C) and heat conduction heat transfer was taken into consideration. In each FEA, the maximum temperature and the stress are monitored in order to be kept under the maximum allowable temperature of 550 °C and yield strength of 7 GPa to avoid any plastic deformation or mechanical failure.

4.1. The optimization of the step feature

The optimization of the step feature is necessary to increase the performance. For this purpose, step length (L_n) and step depth are separately evaluated through multiple FEAs. The expected displacements are calculated based on temperature rise of 530 °C as an external excitation. During this FEA, various L_n have been tested, ranging from 50 to 900 μm. Their corresponding responses are plotted in figure 4(a) where a local maximum displacement of 62 μm is observed at 500 μm step length. With the step length (L_n) of 500 μm, the step depth (e) was also examined through FEA with the same thermal excitation of 530 °C increment. Their corresponding responses are in figure 4(b) where a local maximum of 82 μm is possible with the step depth of 22.5 μm. These values are applied to the step design parameters, allowing displacements of greater than 80 μm.

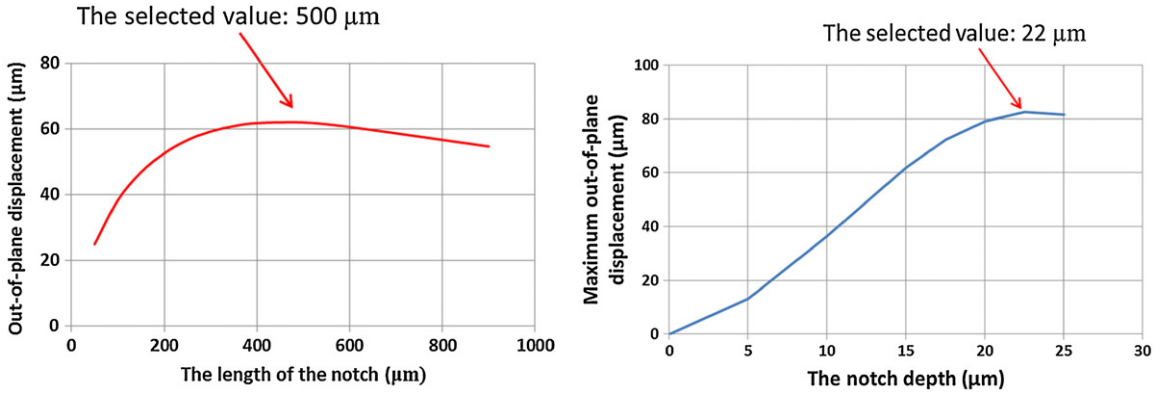

(*a*) (*b*)

Figure 4. (*a*) An out-of-plane displacement as a function of the step length (L_n); (*b*) an out-of-plane displacement as a function of the step depth (*e*).

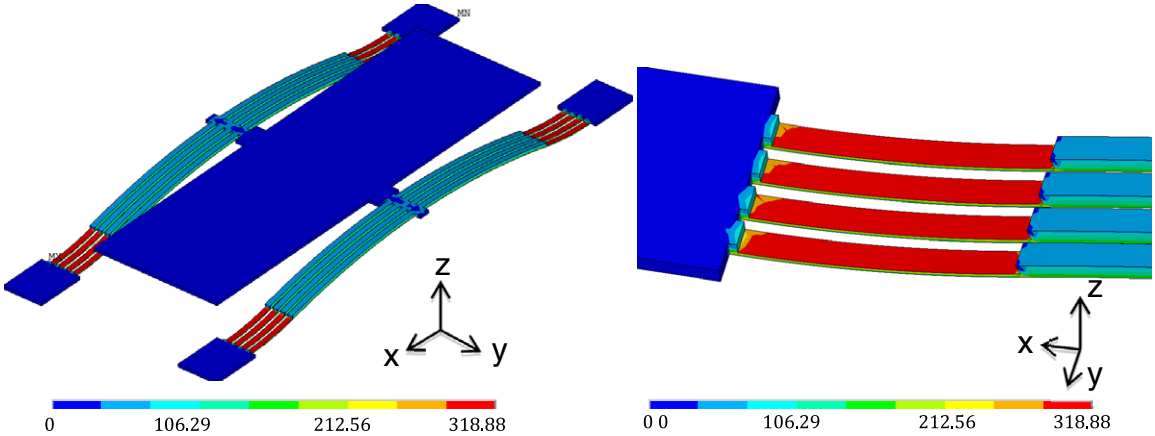

(*a*) (*b*)

Figure 5. Finite element analysis results on von Mises stress distribution on the actuator; (*a*) a full view; (*b*) a close-up view near the step.

4.2. Stress distribution

In order to monitor any mechanical failure during operation, its von Mises stress distribution was calculated when its maximum displacement of 85.1 μm was generated. The response from the stage is shown in figure 5(*a*) where the whole actuator except the step features experiences stress less than 140 MPa. Around the step feature, the maximum stress increases and is found to be 318.9 MPa as depicted in figure 5(*b*). These values imply that the step feature experiences most deformation and can be a bottleneck to limit its maximum. However, the value obtained is still far less than the yield strength of silicon 7 GPa, so no mechanical failure is expected during its normal operations up to 85 μm. Since 94 μm motion produces a stress still less than 500 MPa, the presented stage for 85 μm displacements can operate stably without any mechanical failure or fatigue.

4.3. The frequency response, stiffness and maximum force of the motion stage

The dynamic behavior of the moving stage is also analyzed: three natural frequencies and the corresponding mode shapes. The first mode has a natural frequency of 4.567 kHz and a mode shape of pure translational motion normal to the moving platform. The second and third modes are rocking modes at 8.532 kHz along the *X* axis and at 9.850 kHz along the *Y* axis, respectively. These two modes are at least 80% larger than the first mode, so the presented design provides enough separation between the desired motion and potential parasitic motions.

The stiffness of the motion stage is also calculated under the situation that a 1 μN force is applied to the middle of the moving platform as mechanical excitation. From this, the moving stage is expected to have a stiffness of 128.2 N m^{-1} along the out-of-plane direction. The maximum force from the actuator is calculated under the case that the temperature increment of 530 °C is used as a thermal excitation and the moving platform firmly held at zero displacement as a mechanical constraint. The corresponding result was found to be 13.81 mN. Based on these two values, the ideal maximum displacement is approximately 107.7 μm without considering any thermal or structural limits. These properties obtained from FEA are compared with measured data in section 5.

5. Fabrication

The fabrication process flow is based on the SOI-MUMPs [24] and each process step is described in figure 6. The

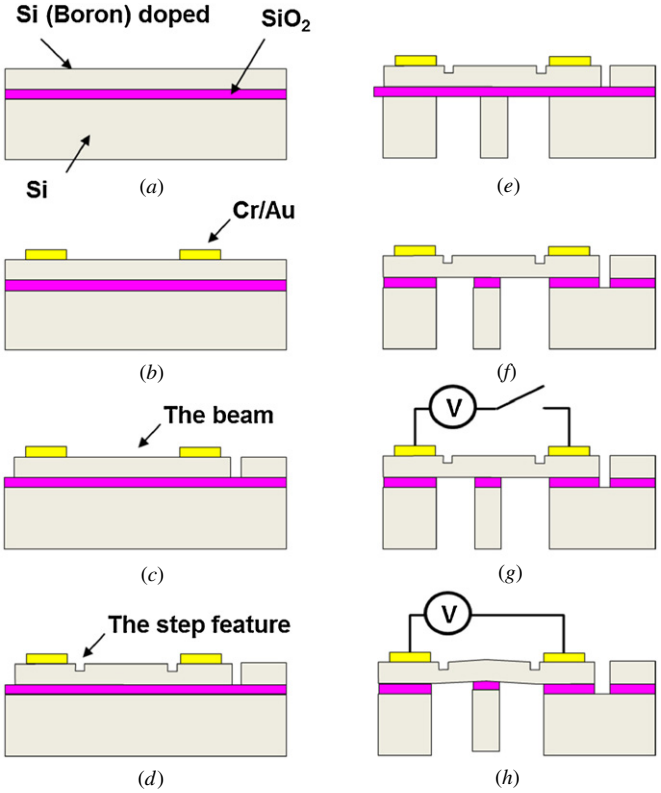

Figure 6. The fabrication flow: (*a*) SOI wafer as a starting material; (*b*) Au/Cr layer deposition for an electrical connection; (*c*) first etching for the beam and the motion stage except for the steps using DRIE; (*d*) second etching for the steps using DRIE; (*e*) etching of the handle layer using DRIE; (*f*) etching the buried oxide layer to release the motion platform; (*g*) electrical connection by wire-bonding; (*h*) an expected deformation during its operation.

device is fabricated on a SOI wafer which is composed of a device layer with a thickness of 30 μm, a buried oxide layer with a thickness of 2 μm and a handle layer with a thickness of 400 μm, as shown in figure 6(*a*). The fabrication process consists of a metal deposition step for generating the electrical connection pads and wires (figure 6(*b*)), the first deep reactive ion etching (DRIE) of the device layer to build the main devices (figure 6(*c*)), the second DRIE to fabricate the step features (figure 6(*d*)) and the third DRIE to form the anchors and the connecting block and to release the main devices for operation (figure 6(*e*)). After these three DRIE steps, a buried oxide layer between the device layer and the handle layer is partially eliminated to make the moving stage free (figure 6(*f*)). All the etching steps are implemented by the Bosch process (Deep RIE-Unaxis SHUTTLELINE DSEII[4]) and the metal deposition step by an electron-beam evaporator (Denton Infinity 22[4]). The fabricated device is connected to external electrical dc actuation voltage for its operation (figure 6(*g*)) and its expected operation is depicted in figure 6(*h*).

Based on the fabrication flow described in figure 6, the presented stage has been successfully fabricated and its captured images from a scanning electron microscope are shown in figure 7. Figure 7(*a*) is the full view of the proposed motion stage where two 'C'-shaped bright areas are metal pads for electrical connection and the gray areas represent the motion stage made of silicon. For reliable fabrication, the moving platform has three holding fingers at each corner that connect the moving platform to the fixed boundary frame during the fabrication and will be released after the fabrication process described in figure 7(*f*). Close-up views for the step feature near the metal pad and the beam are shown in figures 7(*b*) and (*d*), respectively. First and second independent DRIE etching described in figures 6(*c*) and (*d*) create the step features without damaging other features. The connecting block underneath the actuator and the moving platform is shown in figure 7(*c*). This blocking delivers the out-of-plane motion from the actuators to the moving platform and electrically isolates the moving platform from the actuators.

6. Experimental results

In order to assess the static performance of the motion stage, a fringe-counting type optical profiler (VEECO WYKO[4] NT1100) has been used as an out-of-plane displacement sensor. The optical profiler scans a target area and a reference area to generate its depth information and measures the relative position between them to obtain displacement data. This measurement has less than 1 μm error but its measurable range is up to 1 mm which is necessary in this case. The stage is electrically connected to a dc power supply unit (Agilent[4] model 3322A) for its static performance test. Figure 8 shows the measured out-of-plane displacement of the moving platform as a function of the input dc current ranging from 0 to 250 mA. This curve is also compared with the secant curve from equation (1) showing a similar trend. For a current from 40 to 220 mA, the output displacement increases with a constant rate of 0.4 μm mA^{-1}. At 220 mA, the stage generates 85 μm of out-of-plane displacement and a current of 245 mA produces a motion up to 95 μm, but the rate of movement gets smaller after 220 mA. Thus, operation up to 85 μm can be considered stable. No mechanical or thermal failure has been observed during these experiments.

The stiffness of the motion stage was measured using a contact profilometer (Veeco Dektak 6M[4]) varying the pushing force from 1 to 10 mg that yields the value of 138.8 N m^{-1}, which is slightly larger than the value estimated from FEA. From the stiffness and the motion range, the actual force generated from the electrothermal actuator is calculated to be 11.80 mN.

In order to look at the deformation behavior of the beam near its step feature during its operation, its deformation was experimentally scanned during displacement and compared with its original shape. In figure 9(*a*), the deformation profiles are plotted showing that the out-of-plane deformation is well distributed over the step feature. The shape in 3D images is shown in figures 9(*b*) and (*c*). The deformation profile of the middle of the beam was also scanned in figure 9(*d*), showing a smooth concave curve. This concave shape matches up with the estimated shape from equation (1) and FEA. In addition, this shape is completely different from the profile under buckling [30] and indicates that the current beam is not under buckling but pure elastic bending.

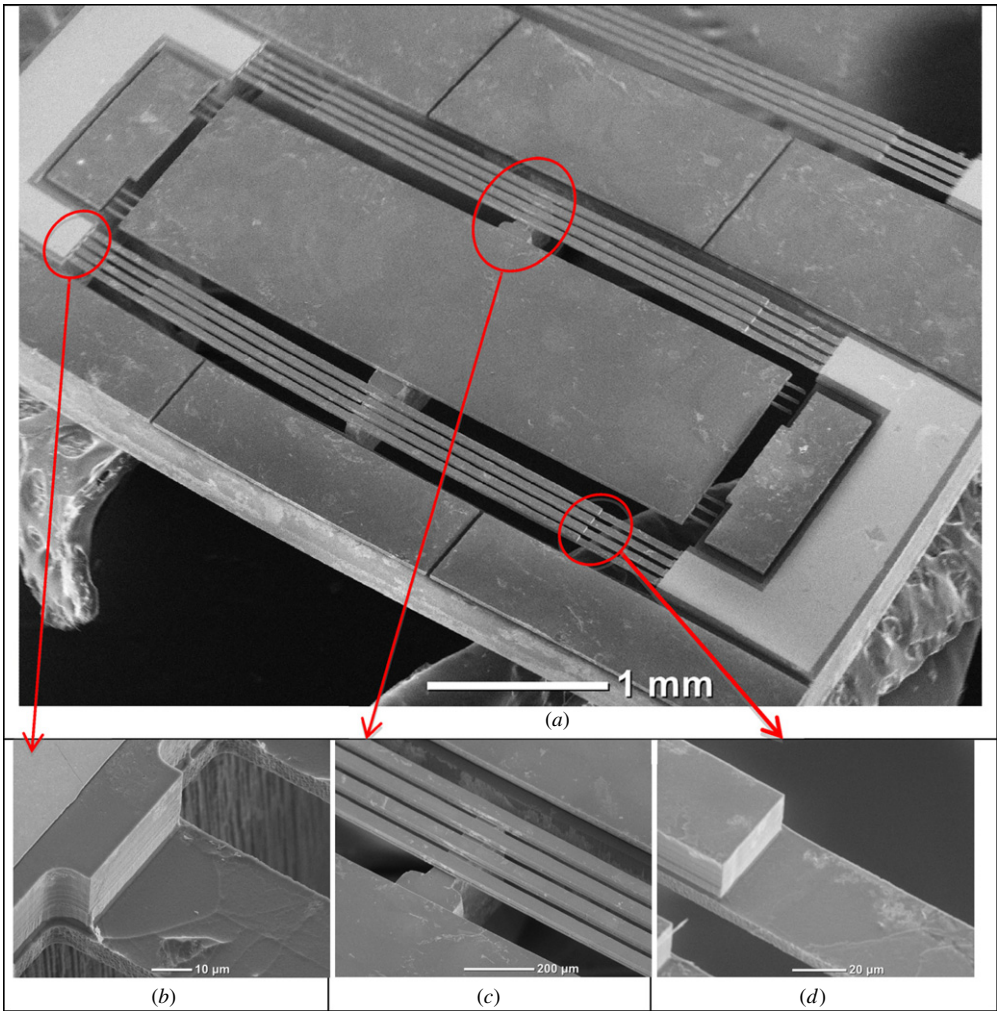

Figure 7. The out-of-plane electrothermal actuator in scanning electron microscope (SEM); (*a*) a full view; (*b*) the sidewall of the step near the metal pad; (*c*) a close-up view of the block connecting the actuator to the platform; (*d*) the sidewall of the step near the beam.

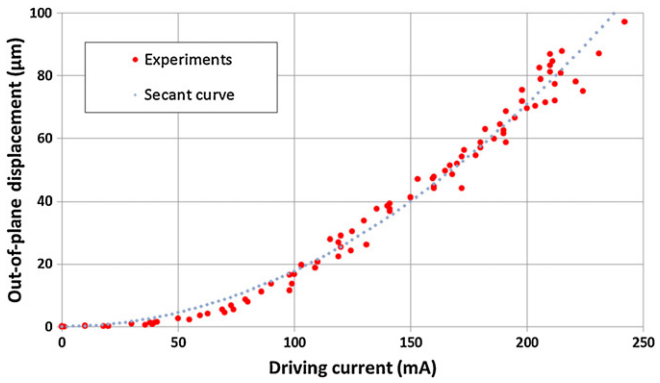

Figure 8. A comparison between the measured out-of-plane motion of the stage and the calculated one.

The dynamic frequency response of the presented motion stage has been measured with a Polytec[4] Micro System Analyzer (MSA-500) [31], which has been mainly used for atomic force microscope applications. From the measurement, the resonant frequencies of the first three modes are measured and found to be 4.41 kHz, 8.00 kHz and 9.72 kHz, respectively. This response is plotted in figure 10, where the frequency range at less than 4 kHz is regarded as white noise from the experimental set-up itself. Each peak has a magnitude high enough to tell the difference, and the first three modes have 1% to 6% differences from the estimated FEA values which are very close to its FEA considering variations and deformations during MEMS fabrication.

The repeatability of the presented system is also quantitatively measured; the stage has been operated more than 1 billion cycles at its natural frequency. The displacements after every 400 k cycles have been measured with three fabricated devices and their results are shown in figure 11(*a*). The stages generate 85 to 90 μm displacements by 220 mA currents and have demonstrated similar displacement after 4×10^5, 8×10^5 and 1.2×10^6 cycles.

The resistance of the actuator was monitored during all experiments and can be used as an indicator of the internal condition of the actuators. Figure 11(*b*) shows the resistance of the actuator as a function of a driving current where the blue solid line is for the stage by an increasing current and the red dotted line is by a decreasing current. This plot shows a slow increase of resistance with an increasing current and a return to its original value after testing. This trend is similar with the measured data [27] and no discontinuous increment has been

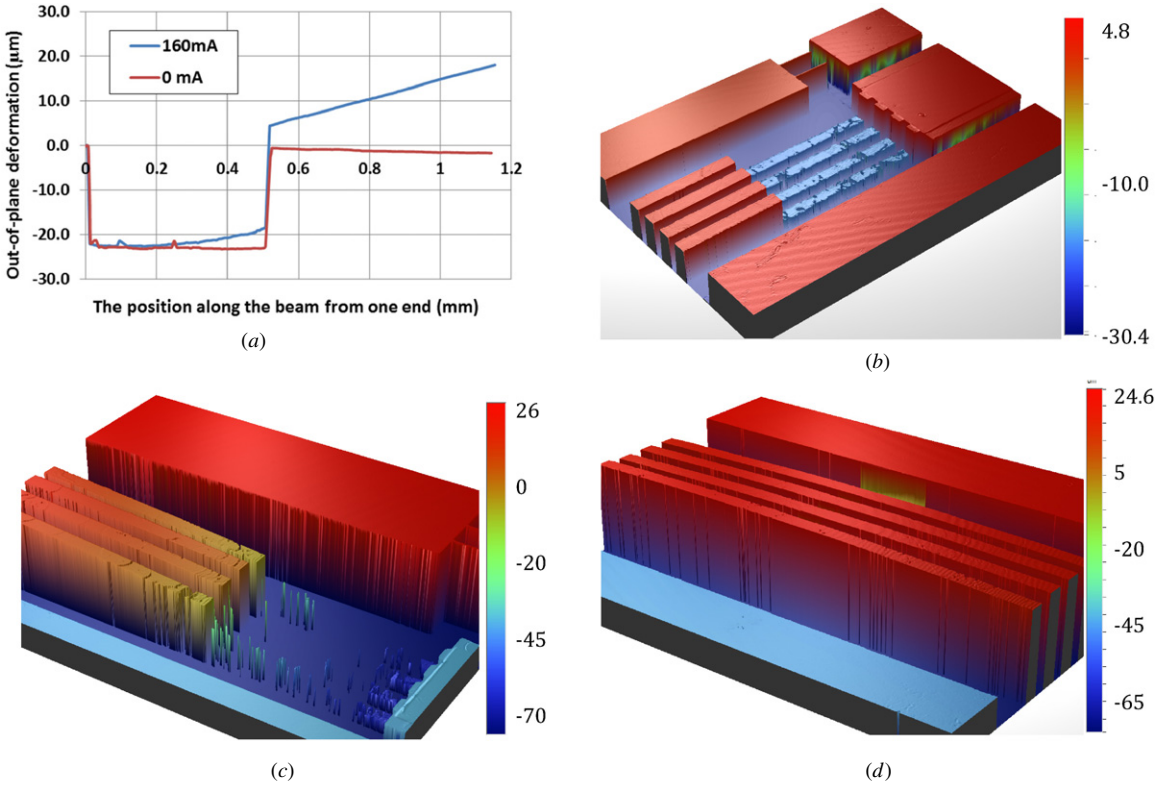

Figure 9. (*a*) Two measured deformation profiles of the step with 0 and 160 mA current; (*b*) a 3D scanned image of the step with 0 mA current; (*c*) a 3D scanned image of the step with 200 mA current; (*d*) a 3D scanned images of the beam at its center with 200 mA current.

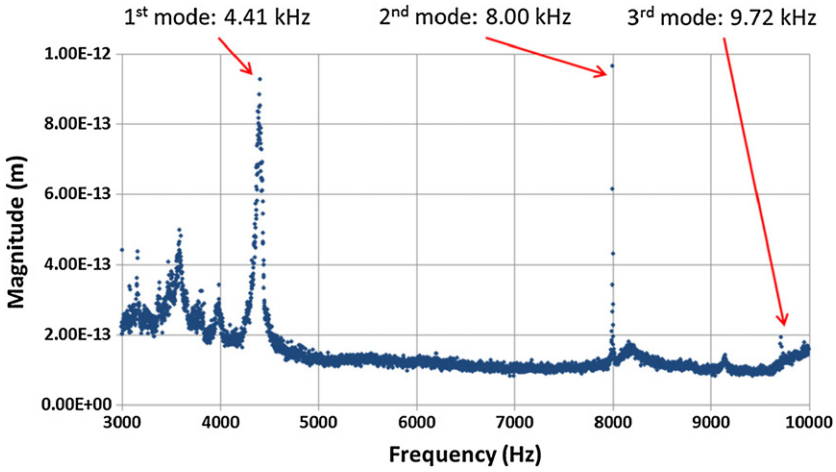

Figure 10. A frequency response of the presented stage.

observed implying no plastic deformation or internal changes occur during its operation.

7. Discussion

The goal of this work is to develop a MEMS motion stage that generates out-of-plane motion and provides a similar range to existing in-plane motion stages. For this purpose, a stiffness larger than tens of N m^{-1}, a few milli-Newton level force, and a motion range of close to 100 μm has been achieved. The similarity of their performance plays an important role in some applications such as collaboration between in-plane and out-of-plane stages or integration of out-of-plane actuation with in-plane actuation. Due to the lack of versatility in MEMS fabrication, MEMS motion stages or manipulators that can be compared with conventional stages fabricated from precision machining are rare. In order to overcome this limit, collaboration between multiple MEMS devices can be a key to improve their performance. As a first step for this purpose, an out-of-plane stage with equivalent performance to in-plane stages is required, because in-plane structures are considerably different from out-of-plane structures in MEMS fabrication approaches.

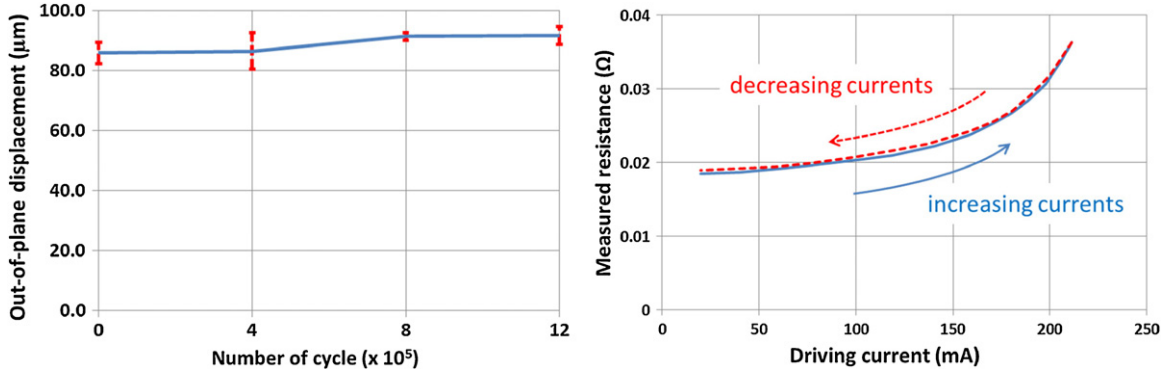

Figure 11. (*a*) A repeatability test over 12 $\times$ 10^5 cycles with (220 to 225) mA driving currents; (*b*) a resistance change as a function of driving currents.

When compared with other in-plane stages, the presented stage with the stiffness of 133 N m^{-1} has a similar level to the selected in-plane stage of 39.5 N m^{-1} [33, 32]. The maximum range of motion is 85 μm, which is larger than 60 μm of the in-plane stage [5]. The expected maximum force of 13 mN is of a comparable level to that of the in-plane stage, which achieves 2–3 mN force. These properties depend mainly on the thick device fabricated through bulk micromachining technologies. This comparison is not meant to claim that the presented stage is better than the target in-plane stage. Rather, it focuses on the fact that the presented stage is designed to provide similar performance or characteristics to the existing in-plane stage, which is an advantage at integration with previous in-plane stages for future collaboration work. Due to this reason, its fabrication method is also limited to the same method as the in-plane stage for easy implementation.

Although the presented motion stage meets the required specifications, there are a few design modifications to increase its usability. As mentioned in the analytic analysis section, the relative position of the step determines the direction of out-of-plane motion. Current design has two step features near the beam ends and generates upward motion. Alternatively, the step feature could be placed in the middle of the beam and therefore generate downward out-of-plane motion. Additionally, the combination of the downward out-of-plane actuator and the upward motion actuator presented in this paper can generate rotational motion of the platform.

8. Conclusions

In this paper, a thermally actuated upward out-of-plane motion stage has been presented with mechanical characteristics at a similar level to in-plane motion stages, especially in terms of motion range, stiffness and maximum force capability. In addition, the fabrication methods for the presented stage have been controlled to be compatible with in-plane motion stages, especially based on electrothermal actuation type and bulk micromachining technologies. The new stage was designed based on the use of a step feature in the beam in order to utilize the eccentric load for out-of-plane motions. This stage has been implemented based on SOI wafers through SOI-MUMPs. The fabricated motion stage has demonstrated an 85 μm range of motion and a maximum force capability of 11.8 mN. The measured properties were found to be in similar ranges to existing in-plane motion stages [5, 32]. These results demonstrate that the presented out-of-plane electrothermal motion stage based on the step feature has potential in extending its role in various applications through collaboration or integration with in-plane stages for a coordinated manipulation or higher degrees-of-freedom motion stages.

Acknowledgments

The authors would like to thank Dr Seung-Ho Yang for his valuable review and Dr Richard Gates for an out-of-plane resonant frequency measurement experiment. This research was performed in part in the NIST Center for Nanoscale Science and Technology Nano Fabrication Clean Room. This work was supported by the Next Generation Robotics and Automation program of the Intelligent Systems Division, Engineering Laboratory, National Institute of Standards and Technology, USA.

References

[1] Beyeler F, Neild A, Oberti S, Bell D J, Sun Y, Dual J and Nelson B J 2007 Monolithically fabricated microgripper with integrated force sensor for manipulating microobjects and biological cells aligned in an ultrasonic field *J. Microelectromech. Syst.* **16** 7–15

[2] Donald B R, Levey C H and Paprotny I 2008 Planar microassembly by parallel actuation of MEMS microrobots *J. Microelectromech. Syst.* **17** 789–808

[3] Jeon C-S, Park J-S, Lee S-Y and Moon C-W 2007 Fabrication and characteristics of out-of-plane piezoelectric micro grippers using MEMS processes *Thin Solid Films* **515** 4901–4

[4] Choi Y-M, Gorman J J, Dagalakis N G, Yang S H, Kim Y and Yoo J M 2012 A high-bandwidth electromagnetic MEMS motion stage for scanning applications *J. Micromech. Microeng.* **22** 105012

[5] Kim Y-S, Yoo J-M, Yang S H, Choi Y-M, Dagalakis N G and Gupta S K 2012 Design and fabrication of a MEMS XY-stage using a serial kinematic mechanism for multi-finger manipulation *J. Micromech. Microeng.* **22** 085029

[6] Physik Instrumente (PI) 2009 P-611.3 NanoCube XYZ Piezo Stage www.physikinstrumente.com/en/products/prdetail.php?sortnr=201700
[7] Liu X, Kim K and Sun Y 2007 A MEMS stage for 3-axis nanopositioninig *J. Micromech. Microeng.* **17** 1796–802
[8] Ando Y 2004 Development of three-dimensional electrostatic stages for scanning probe microscope *Sensors Actuators* A **114** 285–91
[9] Fan L, Wu M C, Choquette K D and Crawford M H 1997 Self-assembled microactuated XYZ stage for optical scanning and alignment *Proc. Int. Conf. Solid-State Sensors and Actuators (Chicago, IL)* pp 319–22
[10] Johnstone R W and Parameswaran M 2001 Self-assembly of surface-micromachined structures using electrostatic attraction *Proc. SPIE* **4561** 66–76
[11] Tsang S H, Sameoto D and Parameswaran M 2006 Out-of-plane electrothermal actuators in silicon-on-insulator technology *Can. J. Electr. Comput. Eng.* **31** 97–103
[12] He S and Mrad R B 2005 Large-stroke microelectrostatic actuators for vertical translation of micromirrors used in adaptive optics *IEEE Trans. Ind. Electron.* **52** 974–83
[13] Wang J, Yang Z and Yan G 2012 Silicon-on-insulator out-of-plane electrostatic actuator with *in situ* capacitive position sensing *J. Micr/Nanolithogr. MEMS MOEMS* **11** 033006
[14] Wagner B and Benecke W 1991 Microfabricated actuator with moving permanent magnet *Proc. Conf. IEEE MEMS* pp 27–32
[15] Cho H J and Ahn C H 2002 A bidirectional magnetic microactuator using electroplated permanent magnet arrays *J. Microelectromech. Syst.* **11** 78–84
[16] Liu C, Tsao T, Lee G-B, Jeremy T, Leu S, Yi Y W, Tai Y-C and Ho C-M 1999 Out-of-plane magnetic actuators with electroplated permalloy for fluid dynamics control *Sensors Actuators* **78** 190–7
[17] Lagorce L K, Brand O and Allen M G 1999 Magnetic microactuators based on polymer magnets *J. Microelectromech. Syst.* **8** 2–9
[18] Atre A 2006 Analysis of out-of-plane thermal microactuators *J. Micromech. Microeng.* **16** 205–13
[19] Chen W C, Yeh P, Hu C F and Fang W 2008 Design and characterization of single-layer step-bridge structure for out-of-plane thermal actuator *J. Microelectromech. Syst.* **17** 70–7
[20] Chen W C, Chu C-C, Hsieh J and Fang W 2003 A reliable single-layer out-of-plane micromachined thermal actuator *Sensors Actuators* A **103** 48–58
[21] Que L, Park J-S and Gianchandani G Y B 2001 Bent-beam electrothermal actuators—part I. Single beam and cascaded devices *J. Microelectromech. Syst.* **10** 247–54
[22] Ogando K, La Forgia N, Zarate J J and Pastoriza H 2012 Design and characterization of a fully compliant out-of-plane thermal actuator *Sensors Actuators* A **183** 95–100
[23] Varona J, Tecpoyoti-Torres M and Hamoui A A 2009 Design of MEMS vertical-horizontal chevron thermal actuators *Sensors Actuators* A **153** 127–30
[24] Cowen A, Hames G, Monk D, Wilcenski S and Hardy B 2008 *SOIMUMPs Design Handbook revision 4.0* www.memscap.com/mumps/documents/SOIMUMPs.dr.v4.pdf
[25] Beer F P and Johnston E R Jr 1992 *Mechanics of Materials* 2nd edn (New York: McGraw-Hill) pp 650–1
[26] Luo J L, Flewitt A J, Spearing S M, Fleck N A and Milne W L 2005 Three types of planar structure microspring electro-thermal actuators with insulating beam constraints *J. Micromech. Microeng.* **15** 1527–35
[27] Baker M S, Plass R A, Headley T J and Walraven J A 2004 Final report: compliant thermomechancial MEMS actuators *Sandia Report* SAND2004-6635 www.mems.sandia.gov/tech-info/doc/thermal_actuator_SAND.pdf
[28] Patel J R and Chaudhuri A R 1963 Macroscopic plastic properties of dislocation-free germanium and other semiconductor crystals *J. Appl. Phys.* **34** 2788–99
[29] Gallagher C J 1952 Plastic deformation of germanium and silicon *Phys. Rev.* **88** 721–2
[30] Johnes R M 2008 *Buckling of Bars, Plates, and Shells* (Blacksburg VA: Bull Ridge) pp 69–72
[31] Polytec MSA-500 Micro System Analyzer www.polytec.com/us/products/vibration-sensors/microscope-based-systems
[32] Bérgna S, Gorman J J and Dagalakis N G 2005 Design and modeling of thermally actuated MEMS nanopositioners *IMECE2005: ASME Int. Mechanical Engineering Congr. and Exp. (Orlando, FL)* IMECE2005-82158
[33] Yang S H, Kim Y, Purushotham K P, Yoo J-M, Choi Y-M and Dagalakis N 2010 AFM characterization of nanopositioner in-plane stiffness *Sensors Actuators* A **163** 383–7